

RESEARCH

Open Access



# Dysregulated ATX-LPA and YAP/TAZ signaling in dystrophic *Sgcd*<sup>-/-</sup> mice with early fibrosis and inflammation

Cristian Gutiérrez-Rojas<sup>1,2,3\*</sup>, Adriana Córdova-Casanova<sup>3</sup>, Jennifer Faundez-Contreras<sup>3,4</sup>, Meilyn Cruz-Soca<sup>3</sup>, Felipe S. Gallardo<sup>3</sup>, Alexia Bock-Pereda<sup>3</sup>, Juan Carlos Casar<sup>5</sup>, Elisabeth R. Barton<sup>6</sup> and Enrique Brandan<sup>3,4\*</sup>

## Abstract

**Background** Sarcoglycanopathies are muscle dystrophies caused by mutations in the genes encoding sarcoglycans ( $\alpha$ ,  $\beta$ ,  $\gamma$ , and  $\delta$ ) that can destabilize the dystrophin-associated glycoprotein complex at the sarcolemma, leaving muscle fibers vulnerable to damage after contraction, followed by inflammatory and fibrotic responses and resulting in muscle weakness and atrophy. Two signaling pathways have been implicated in fibrosis and inflammation in various tissues: autotaxin/lysophosphatidic acid (ATX-LPA) and yes-associated protein 1/transcriptional co-activator with PDZ-binding motif (YAP/TAZ). LPA, synthesized by ATX, can act as a pleiotropic molecule due to its multiple receptors. Two Hippo pathway effectors, YAP/TAZ, can be dephosphorylated by LPA and translocated to the nucleus. They induce several target genes, such as CCN2/CTGF, involved in fibrosis and inflammation. However, no detailed characterization of these processes or whether these pathways change early in the development of sarcoglycanopathy has been evaluated in skeletal muscle.

**Methods** Using the  $\delta$ -sarcoglycan knockout mouse model (*Sgcd*<sup>-/-</sup>), we investigated components of these pathways, inflammatory and fibrotic markers, and contractile properties of different skeletal muscles (triceps-TR, gastrocnemius-GST, diaphragm-DFG, tibialis anterior-TA, and extensor digitorum longus-EDL) at one and two months of age.

**Results** We found that *Sgcd*<sup>-/-</sup> mice show early dystrophic features (fiber damage/necrosis, centrally nucleated fibers, inflammatory infiltrate, and regenerated fibers) followed by later fiber size reduction in TR, GST, and DFG. These changes are concomitant with an early inflammatory and fibrotic response in these muscles. *Sgcd*<sup>-/-</sup> mice also have early impaired force generation in the TA and EDL, and resistance to mechanical damage in the EDL. In addition, an early dysregulation of the ATX-LPA axis and the YAP/TAZ signaling pathway in the TR, GST, and DFG was observed in these mice.

**Conclusions** The ATX-LPA axis and the YAP/TAZ signaling pathway, which are involved in inflammation and fibrosis, are dysregulated in skeletal muscle from an early age in *Sgcd*<sup>-/-</sup> mice. These changes are concomitant with a fibrotic and inflammatory response in these mice. Unraveling the role of the LPA axis and YAP/TAZ in sarcoglycanopathy holds great promise for improving our understanding of disease pathogenesis and identifying novel therapeutic targets for this currently incurable group of muscle disorders.

\*Correspondence:

Cristian Gutiérrez-Rojas  
cristian.gutierrez@pucv.cl  
Enrique Brandan  
enrique.brandan@uss.cl

Full list of author information is available at the end of the article



© The Author(s) 2025. **Open Access** This article is licensed under a Creative Commons Attribution-NonCommercial-NoDerivatives 4.0 International License, which permits any non-commercial use, sharing, distribution and reproduction in any medium or format, as long as you give appropriate credit to the original author(s) and the source, provide a link to the Creative Commons licence, and indicate if you modified the licensed material. You do not have permission under this licence to share adapted material derived from this article or parts of it. The images or other third party material in this article are included in the article's Creative Commons licence, unless indicated otherwise in a credit line to the material. If material is not included in the article's Creative Commons licence and your intended use is not permitted by statutory regulation or exceeds the permitted use, you will need to obtain permission directly from the copyright holder. To view a copy of this licence, visit <http://creativecommons.org/licenses/by-nc-nd/4.0/>.

**Keywords**  $\delta$  Sarcoglycanopathy, Autotaxin, Lysophosphatidic acid, Fibrosis, Inflammation, Muscle regeneration, Muscle mechanics, YAP/TAZ

## Introduction

Limb-girdle muscular dystrophies (LGMDs) are a group of rare diseases that cause weakness and atrophy of the pelvic and scapular girdle muscles [1, 2]. As genetic diseases, LGMDs result from protein defects along the muscle fiber, including the nucleus, sarcoplasm, sarcomere, sarcolemma, and extracellular matrix (ECM) [3, 4]. The dystrophin-associated glycoprotein (DGC) complex within the muscle fibers establishes a physical link between the ECM and its contractile components. This link provides a shock-absorbing connection, stabilizes the muscle fiber against mechanical forces during contraction [5], and enables cell signaling and trafficking [4]. The DGC is particularly affected in some LGMDs [4]. Sarcoglycanopathies are among the most common recessive LGMDs [6]. They are caused by mutations in genes encoding  $\alpha$ -,  $\beta$ -,  $\gamma$ -, and  $\delta$ -sarcoglycans [7]. As a crucial component of the DGC, mutations in any of the sarcoglycan proteins destabilize the entire sarcoglycan complex at the sarcolemma. Like other dystrophies, the muscle undergoes recurrent cycles of necrosis and regeneration, an inflammatory process, replacement of its fibers by ECM in a phenomenon called fibrosis, and changes in fiber size [1, 8–10]. No detailed characterization of these pathophysiological processes has been reported during the first months of sarcoglycanopathy development. Some alterations have been shown in the calf, thigh, and diaphragm (DFG) [11], but no description in the triceps (TR) muscle has been reported at an early stage. The TR is a muscle with a direct connection to the scapular girdle, making it more representative of the pattern of muscular compromise seen in sarcoglycanopathies [12].

The autotaxin-lysophosphatidic acid (ATX-LPA) axis has become relevant due to the involvement of a signaling lipid in physiological and pathological processes. ATX is a phospholipase that can synthesize LPA from lysophospholipids of the outer leaflet of the plasma membranes [13–15]. This signaling lipid functions predominantly as an extracellular mediator by stimulating cognate G-coupled protein receptors (LPA<sub>1–6</sub>) [14, 16]. LPA signaling is involved in cell migration, cell proliferation, cytoskeletal reorganization, and developmental processes, among many others [17–20]. In contrast, LPA has also been associated with pain, obesity, cardiovascular disease, cancer, fibrosis, and inflammation in various organs, including the liver, kidney, lung, and brain [16, 21–24]. Recently, one of the precursor molecules of LPA, phosphatidylcholine [25], was found

to be altered in *mdx* dystrophic muscles and muscles undergoing regeneration after barium chloride injections [26]. Our group hypothesized that the axis may be involved in the inflammatory and fibrotic responses observed in skeletal muscle diseases [27]. Indeed, components of the axis are present in skeletal muscles of wild-type mice (with LPA<sub>1</sub> and LPA<sub>6</sub> being the most highly expressed receptors), which respond with matrix deposition after LPA challenge [28]. While many of the identified mediators and pathways in muscle dystrophies are predominantly protein, the role of specific lipid pathways, such as the ATX-LPA axis in sarcoglycanopathies, remains largely unexplored. Deciphering the role of the LPA axis in sarcoglycanopathy holds significant promise for improving our understanding of disease pathogenesis and identifying novel therapeutic targets for this currently incurable group of muscle disorders.

LPA can act as a pleiotropic molecule due to its multiple receptors with different expression patterns and diverse effectors. Two effectors are Yes-associated protein 1 (YAP) and transcriptional co-activator with PDZ-binding motif (TAZ), part of the kinase cascade known as the Hippo pathway. YAP/TAZ are involved in fibrosis of various tissues [29], including skeletal muscle [30]. For instance, enhanced YAP/TAZ expression has been observed in fibrotic lung tissue [31]. Both proteins are also critical regulators of hepatic fibrogenesis driven by hepatic stellate cell activation [32]. YAP is a crucial regulator of tubulointerstitial fibrosis during the transition to chronic kidney disease [33]. Moreover, cross-talk between Hippo-YAP and the inflammatory pathways has been reported, an interaction that depends on the cell type and disease context [34]. For example, TAZ has been shown to promote liver inflammation by increasing the secretion of pro-inflammatory cytokines. Similarly, an active form of YAP expressed in mouse hepatocytes strongly enhances the secretion of TNF $\alpha$  and IL-1 $\beta$ . In contrast, hepatocyte-specific YAP or YAP/TAZ knockouts (KO) displayed reduced inflammation [35]. In the skeletal muscle, LPA is able to promote YAP dephosphorylation, its translocation to the nucleus, and the induction of different Hippo pathway target genes, such as Cellular communication network factor 1 (CCN1/Cyr61) and CTGF/CCN2 [25, 28]. Recently, we found that LPA induces YAP dephosphorylation in fibro-adipogenic progenitors (FAPs) and that CTGF induction can be blocked by preventing

YAP transcriptional activity [36]. Denervation also induces muscle fibrosis with YAP/TAZ expression and transcriptional activity, but an increased expression of YAP that accumulates in the nuclei of FAPs [30]. However, no studies have determined the early fibrotic and inflammatory profile of  $\delta$ -sarcoglycanopathy and whether this is concomitant with YAP/TAZ expression.

Here, we report for the first time in TR muscle and also in gastrocnemius (GST) and DFG that mice with  $\delta$  sarcoglycanopathy show early (at the first month) features of dystrophy, fibrosis, inflammation, and regenerative foci, followed by later (at the second month) fiber size reduction. In addition, reduced force generation, fatigue tolerance, and mechanical damage resistance are present from an early stage of development. Finally, dysregulation of the ATX-LPA axis and the YAP/TAZ pathway is observed, which may be directly involved in

the concomitant inflammatory and fibrotic response observed early in this dystrophic model.

## Results

### *Sgcd*<sup>-/-</sup> mice show early dystrophic features

To observe how muscles are compromised by delta sarcoglycanopathy, muscles were stained using Hematoxylin & Eosin (H&E) (Fig. 1A). Besides the most studied muscles in muscular dystrophy, DFG and GST, we included TR in the evaluation because of its direct connection to the shoulder girdle and as a representative muscle of LGMD. As early as one month of age, muscle structure was compromised in *Sgcd*<sup>-/-</sup> compared to wild-type mice. Areas of fibers in degeneration (necrosis), fibrosis (increased inter-fiber space), inflammatory infiltrate, and regenerated fibers (fiber with a central nucleus) of different sizes were observed across muscle's sections (Fig. 1B). In the

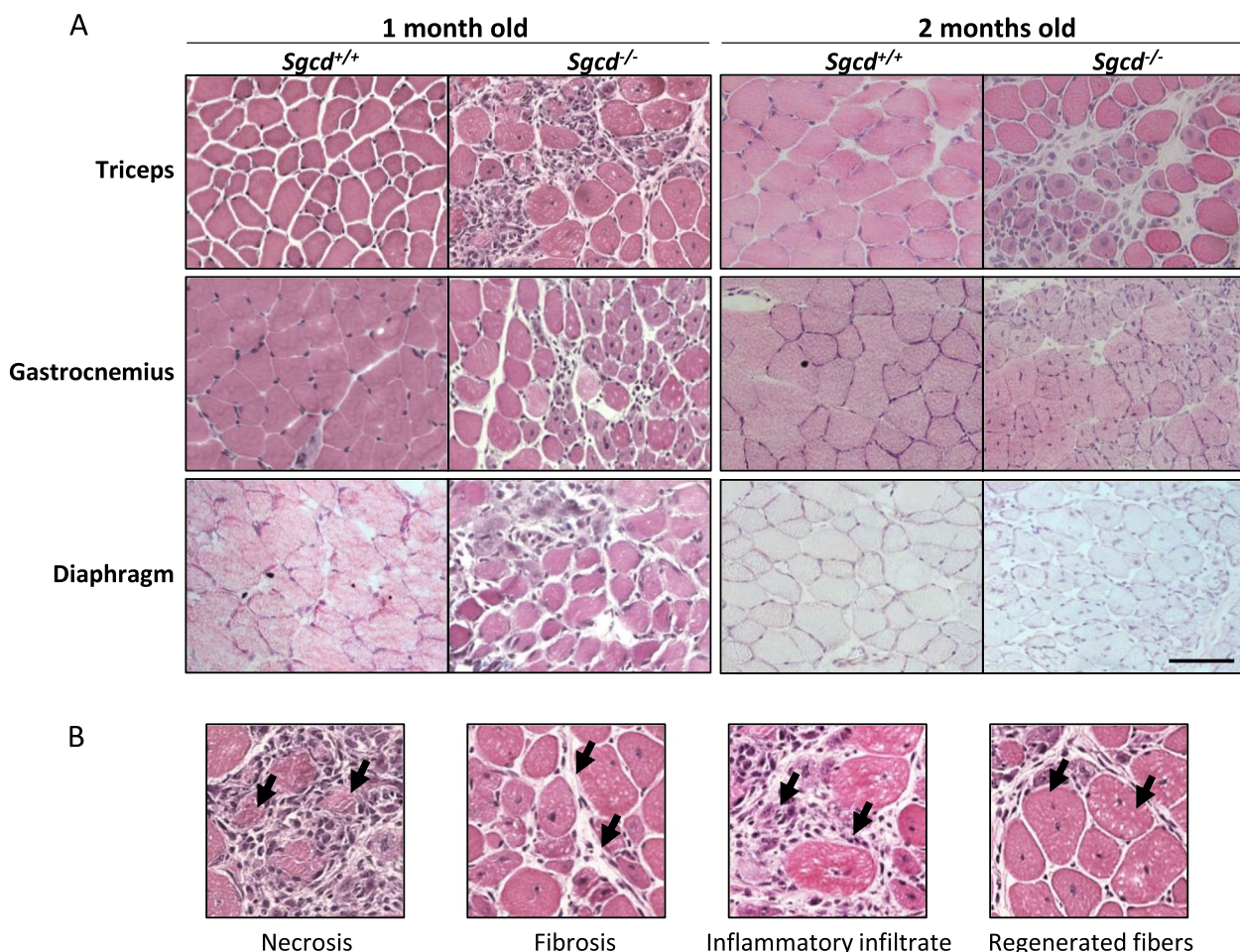


**Fig. 1** *Sgcd*<sup>-/-</sup> mice exhibit early dystrophic features compared to *Sgcd*<sup>+/+</sup> mice. **A** Representative H&E images of skeletal muscle from one- and two-month-old mice. Scale bar: 100  $\mu$ m. **B** Representative images of dystrophic features observed in the TR muscle of one-month-old *Sgcd*<sup>-/-</sup> mice. Image properties (brightness and contrast) have been modified to highlight specific features

second month, the pathological changes became more prominent. This is the first time that the early dystrophic changes in TR have been described in detail and confirm the changes seen in GST and DFG in delta sarcoglycanopathy [11].

#### Early regeneration is followed by later fiber size changes in *Sgcd*<sup>-/-</sup> mice

A feature of muscular dystrophy is a higher proportion of smaller muscle fibers [37]. Since fibers of different sizes were observed in H&E staining at both ages, the minimum Feret's diameter was measured (Fig. 2A). During the first month, virtually no differences were observed in the three muscles studied. However, by the second month, most fibers in *Sgcd*<sup>-/-</sup> mice (~52%) consisted of smaller fibers with a minimum Feret's diameter between 5–20 μm. In contrast, most fibers in *Sgcd*<sup>+/+</sup> mice (~80%) consisted of fibers greater than 20 μm in diameter. In *Sgcd*<sup>-/-</sup> TR, a significant reduction in fiber diameter was observed in almost all diameter classes. In GST, a significant reduction in fiber diameter was observed between the 10–15 and 30–40 μm classes, and DFG, showed a significant reduction in fiber diameter between the 10–15 and 25–35 μm classes (Table S1).

Another characteristic of muscular dystrophy is the presence of fibers undergoing regeneration. *Myh3* gene expression and embryonic myosin heavy chain (eMHC) protein levels were evaluated (Fig. 2B). *Myh3* expression was up-regulated in all muscles of *Sgcd*<sup>-/-</sup> mice at both ages, an expression that decreased in GST and DFG by the second month (Fig. 2B superior panel). As expected, wild-type mice expressed very low levels of this marker. In addition, there was a significant increase in eMHC protein levels at both ages in TR and DFG. However, GST only showed a significant increase in eMHC at two months of age (Fig. 2B inferior panel). To further corroborate the increase in fiber regeneration, laminin/Hoechst (Fig. 2C) and eMHC/laminin (Fig. 2D) indirect immunofluorescence (IIF) were performed in the TR muscle. A significant increase in the percentage of centrally nucleated fibers was observed in the *Sgcd*<sup>-/-</sup> mice at both ages

(Fig. S1 A). A similar result was observed for the percentage of eMHC-positive fibers (Fig. S1 B).

These results reveal that the absence of delta sarcoglycan causes dystrophic muscle changes detectable early (one month of age) in this animal model. The observed muscle damage is followed by early regeneration events that fail to maintain muscle fiber size at two months of age.

#### *Sgcd*<sup>-/-</sup> mice show early inflammatory markers

Muscle damage is accompanied by a physiological inflammatory response necessary for normal muscle regeneration. In contrast, fiber damage is followed by an inflammatory process that becomes maladaptive in muscle dystrophy context [38]. Gene expression levels of molecular (pro-inflammatory cytokines, i.e., *Tnfa*, *Il1b* and *Il6*) and cellular markers (i.e. *Ptprc*, *Ly6c1* and *Mrc1*) were performed to determine how relevant inflammation is in this dystrophic model (Fig. 3A). Among the pro-inflammatory cytokine genes, *Sgcd*<sup>-/-</sup> mice expressed significantly higher levels of *Il1b*, *Tnfa* and *Il6* in all muscles at both ages.

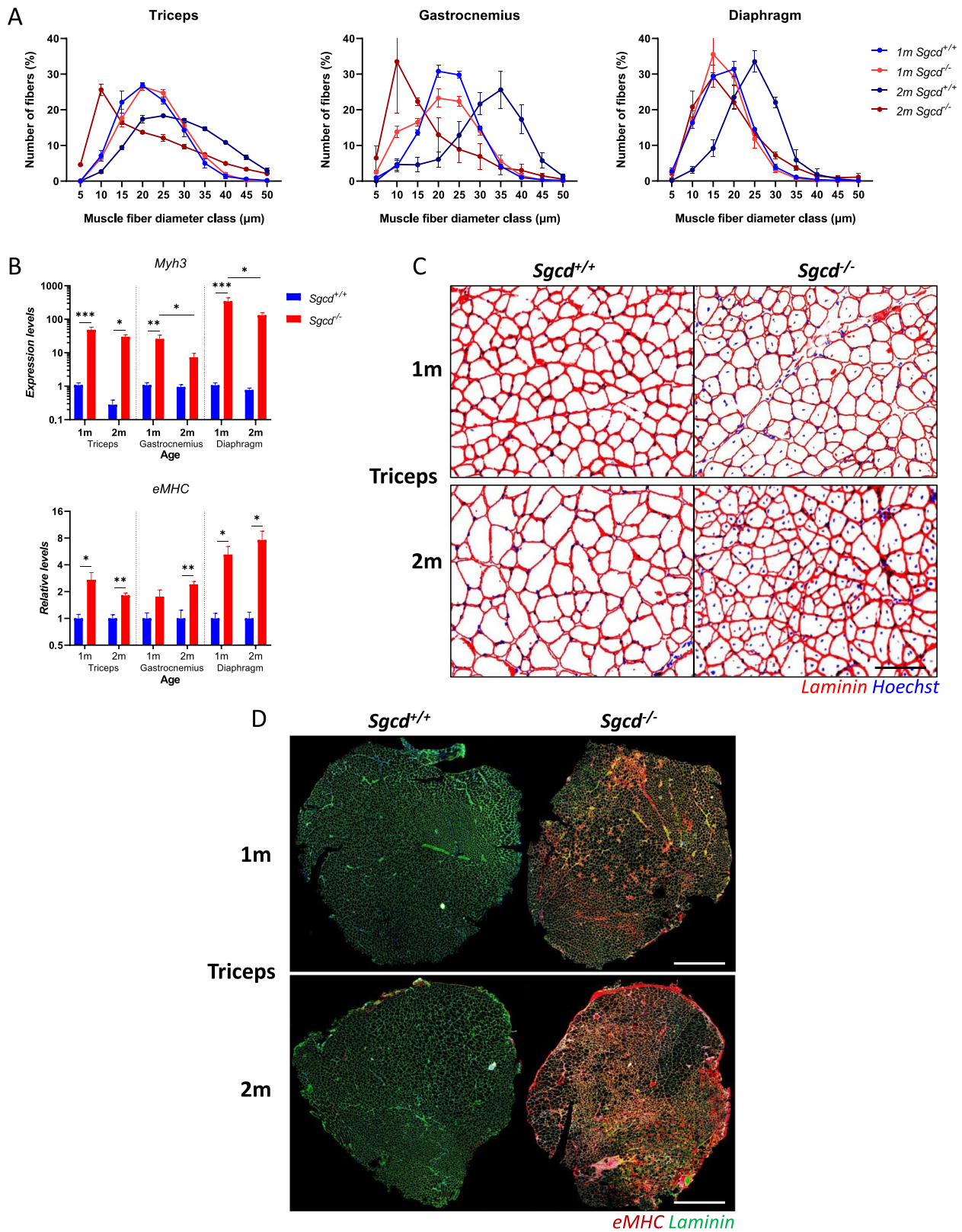
In addition, the *Ptprc* gene for cluster of differentiation 45 (CD45), a hematopoietic cell marker, was significantly increased in *Sgcd*<sup>-/-</sup> mice in both months for TR, GST, and DFG. *Ly6c1*, a gene related to M1 macrophages, was up-regulated in *Sgcd*<sup>-/-</sup> mice during the first month in the DFG and during the second month in the GST and TR. On the other hand, *Mrc1* (a gene related to M2 macrophages) was up-regulated in *Sgcd*<sup>-/-</sup> mice during the second month in TR and GST, but only during the first month in DFG.

CD11b and CD44, markers of monocytes/Macrophages (MPs) and T cells were also evaluated in the TR muscle by IIF. Both of these markers (Fig. 3B) showed a significant increase in the area of fluorescence in the muscle sections (Fig. S2 A and B).

Taken together, *Sgcd*<sup>-/-</sup> mice exhibit features of an enhanced early inflammatory process mediated by molecular and cellular factors, indicating the involvement of the innate and adaptive immune systems.

(See figure on next page.)

**Fig. 2** *Sgcd*<sup>-/-</sup> mice exhibit early (1 month) regeneration followed by later (2 months) fiber size reduction. **A** Fiber size distribution measured by minimum Feret's diameter in laminin-stained muscle sections. Values represent the percentage of fibers (mean ± SEM) in a given diameter class (5 μm/class). Mice were compared at different ages using two-way ANOVA with Tukey's multiple comparisons post-test ( $n=3$ ; Supplementary Table 1). **B** Measurement of *Myh3* gene expression and eMHC protein levels. Data are normalized to *gapdh* ( $n=3-5$ ) and GAPDH ( $n=3$ ), respectively. A two-way ANOVA with Tukey's multiple comparison post-test and an unpaired two-tailed t-test were used to compare genotypes of mice at each age and muscle for gene and protein expression, respectively. Values represent mean ± SEM; \* $p \leq 0.05$ , \*\* $p \leq 0.01$ , and \*\*\* $p \leq 0.001$ . **C** Representative immunofluorescence images of centrally nucleated TR fibers stained with laminin (fibers, red) and Hoechst (nuclei, blue). Scale bar: 100 μm. **D** Representative immunofluorescence images of regenerated TR fibers stained with embryonic myosin heavy chain (eMHC, red) and laminin (green). one-month Scale bar: 1000 μm; two-month Scale bar: 1250 μm



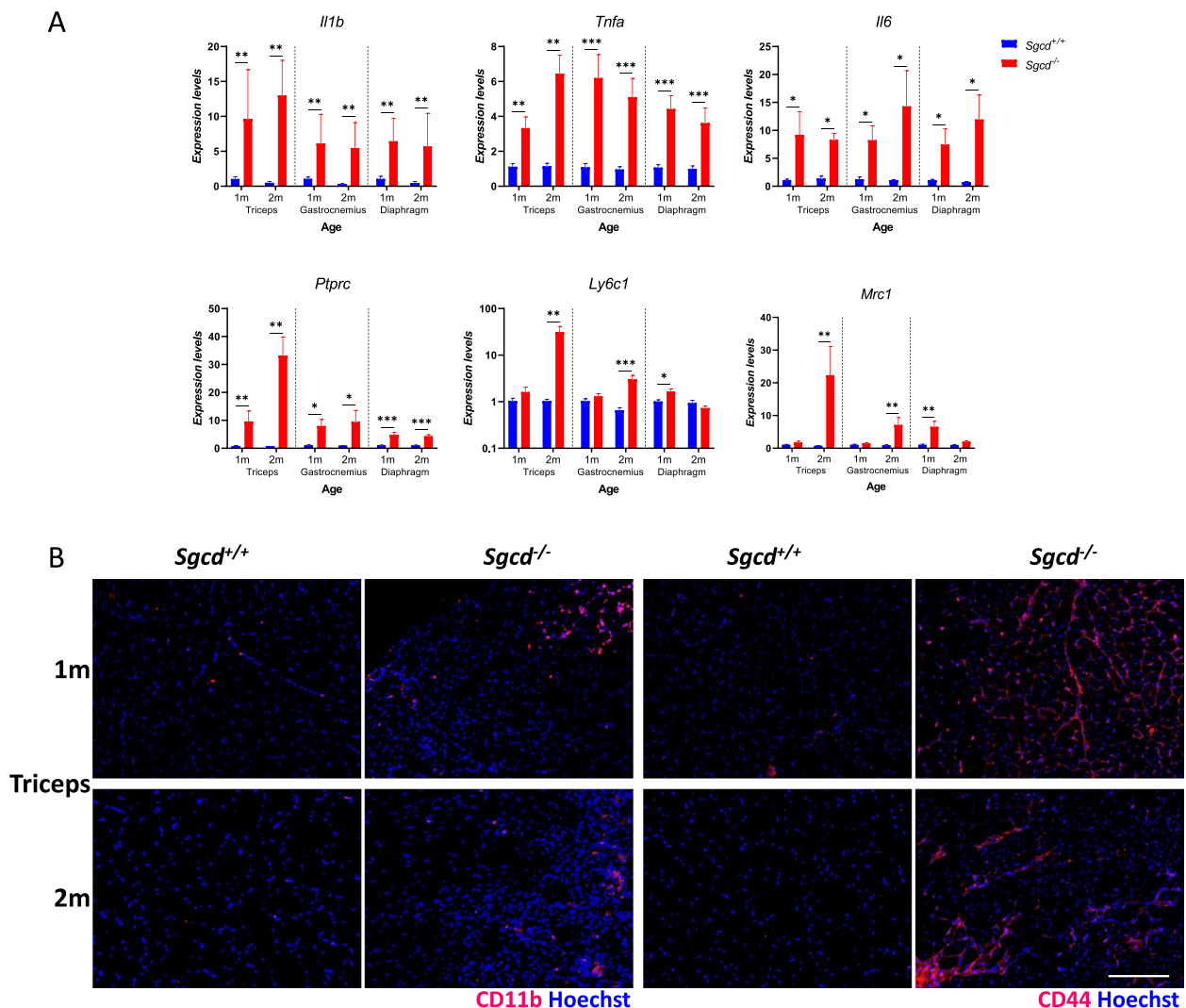


**Fig. 3** Molecular and cellular markers of inflammation are detected early in *Sgcd*<sup>-/-</sup> mice. **A** Gene expression levels of inflammatory cytokines (*Tnfa*, *Il1b*, and *Il6*) and cellular markers (*Ptprc*, *Ly6c1*, and *Mrc1*) are detected early in *Sgcd*<sup>-/-</sup> mice. Data are normalized to *gapdh* (n = 3–5). A two-way ANOVA with Tukey's multiple comparison post-test was used to compare genotypes of mice at each age and muscle. Values represent mean ± SEM; \**p* ≤ 0.05, \*\**p* ≤ 0.01, and \*\*\**p* ≤ 0.001. **B** Representative immunofluorescence images of CD11b (monocyte/MPs marker) and CD44 (T-cell marker) in TR stained with the corresponding antibody (red) and Hoechst (nuclei, blue). Scale bar: 100 μm

### Markers of fibrosis are detected at an early stage in *Sgcd*<sup>-/-</sup> mice

Fibrosis is another hallmark of muscle dystrophies [39], and it is characterized by an excessive ECM accumulation in the replacement of damaged fibers [8, 40, 41] due to excessive matrix synthesis, poor degradation, or both [42]. Fibrosis was examined by gene expression of ECM components (i.e., *Fn1*, *Ccn2*, *Col1a1*, and *Col3a1*) and FAPs/active fibroblast markers, cells responsible for the ECM synthesis (i.e., *Pdgfra* and *Postn*) (Fig. 4A). *Fn1* expression was significantly increased in *Sgcd*<sup>-/-</sup> mice at both ages. During the second month, *Ccn2* (CTGF) expression was upregulated in *Sgcd*<sup>-/-</sup> animals for TR and

DGF muscles. In GST, *Ccn2* upregulation was observed only in the first month. *Col1a1* was significantly increased in *Sgcd*<sup>-/-</sup> mice in the second month for the GST and TR, and in both months for the DFG. The expression levels of *Col3a1* in *Sgcd*<sup>-/-</sup> mice were increased in the second month for TR and in both months for GST and DFG. During the second month in TR and GST, *Pdgfra* expression was up-regulated in *Sgcd*<sup>-/-</sup> mice. No changes were detected in DGF. Increased expression of *Postn* was observed in *Sgcd*<sup>-/-</sup> animals of both ages in the GST and the DFG, but only during the first month in the TR.

Changes in protein levels for ECM components (fibronectin and CTGF) and FAPs/active fibroblast

markers (PDGFR $\alpha$  and periostin) were also determined (Fig. 4B and Fig. S3 A). Fibronectin levels were higher in *Sgcd*<sup>-/-</sup> mice at both ages in TR, but only at the second month in GST and DFG. CTGF protein levels were increased in the first month in the DFG and the second month in TR. Unexpectedly, the levels of this protein were initially reduced in the GST of *Sgcd*<sup>-/-</sup> mice, a trend that was reversed by the second month. Protein levels of PDGFR $\alpha$ , a marker of FAPs, were elevated in all muscles of *Sgcd*<sup>-/-</sup> mice at both ages. The active fibroblast marker periostin only showed a significant increase in *Sgcd*<sup>-/-</sup> mice at two months of age in the TR and GST.

To observe matrix remodeling in TR muscle, fibronectin and collagen were stained with IIF and Sirius Red, respectively (Fig. 4C). *Sgcd*<sup>-/-</sup> mice showed significantly more areas of fluorescence for fibronectin and total collagen deposition than *Sgcd*<sup>+/+</sup> mice at both ages (Fig. S3 B).

These results show an early dysregulation of reparative mechanisms (such as FAPs involvement) that ultimately exacerbate ECM deposition or fibrosis in response to the damage associated with delta sarcoglycanopathy.

#### Force generation and mechanical damage resistance are compromised in *Sgcd*<sup>-/-</sup> mice

Considering that one of the most important functions of muscles is the generation of force and movement and that the assessment of strength is the gold standard for measuring the physiological function of skeletal muscle [43], we evaluated the contractile properties of the tibialis anterior (TA) and extensor digitorum longus (EDL) muscles in sarcoglycanopathy. TA muscle function was assessed by specific isometric force (force-frequency relationship) and fatigue tolerance (fatigue resistance and recovery) in the first and second months of life. At both ages, *Sgcd*<sup>-/-</sup> animals significantly reduced the ability to generate force from 60–200 Hz (Fig. 5A). No differences were found during the fatigue and recovery protocol at either age (Fig. 5B).

Additionally, ex vivo EDL muscle function measurements were performed. EDL muscles from *Sgcd*<sup>-/-</sup> mice had significantly lower specific and normalized forces at 1- and 2-months of age (Fig. 5C). In addition, these mice had a significant decrease in the percentage of force after

subsequent eccentric contractions (ECC) at both ages (Fig. 5D).

These findings indicate that delta sarcoglycanopathy affects muscle contractile properties, reducing the ability to generate force and resist contraction-induced mechanical damage from an early age.

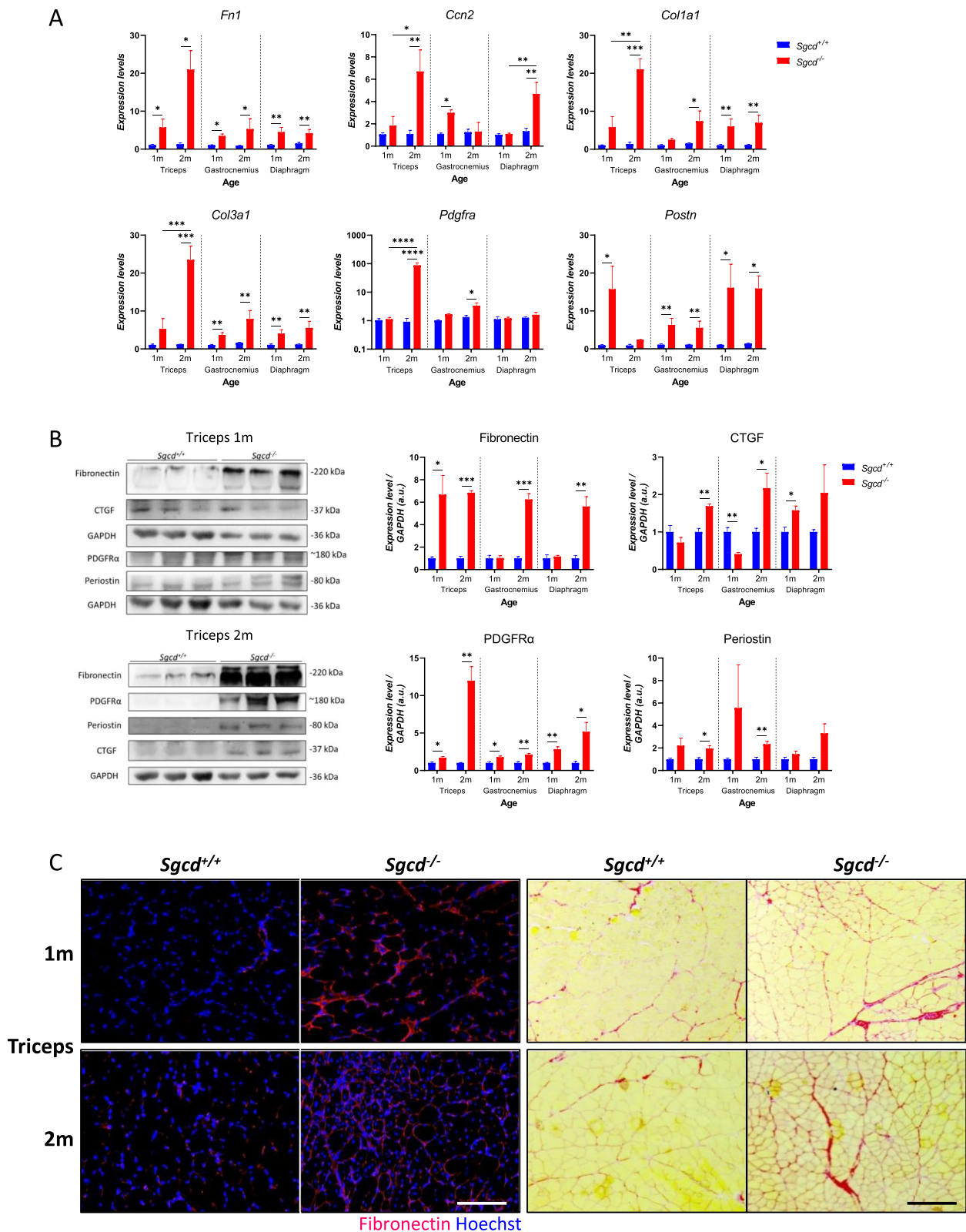
#### The ATX-LPA axis and YAP/TAZ signaling are dysregulated in *Sgcd*<sup>-/-</sup> mice

Since the ATX-LPA axis has been implicated in pathological processes such as fibrosis and inflammation [16, 21–24], and that skeletal muscle expresses its components and also responds to LPA by increasing ECM [28], a temporal characterization of ATX (*Enpp2*), LPA levels and lysophosphatidic acid receptors (LPARs) expression during the development of sarcoglycanopathy  $\delta$  was performed during the first two months of life. Analysis revealed a differential pattern of ATX mRNA expression in  $\delta$  sarcoglycanopathy (Fig. 6A). In the GST, expression was significantly up-regulated at both ages. In contrast, ATX gene expression and levels (by ELISA; Fig. S4 A) were significantly decreased in the TR of 2-month-old *Sgcd*<sup>-/-</sup> mice. No differences were observed in DFG muscle in this model at either age. Furthermore, during the first month of life, *Sgcd*<sup>-/-</sup> mice had elevated levels of LPA in the triceps muscle compared to *Sgcd*<sup>+/+</sup> mice (Fig. 6B). However, no differences were observed in the second month. A dysregulation of the most abundant LPARs in muscle was detected in *Sgcd*<sup>-/-</sup> mice (Fig. 6C). The expression of LPA<sub>1</sub> and LPA<sub>6</sub> was significantly up-regulated in the studied muscles, but at different times. LPA<sub>6</sub> changed from an early stage and LPA<sub>1</sub> changed at the second month. On the other hand, no changes in LPA<sub>2–5</sub> expression were observed.

LPA can signal downstream of its receptors through an effector couple known as YAP/TAZ [44], which has been implicated in the fibrosis of multiple organs [30]. We recently showed in muscle FAPs that phosphorylated YAP is decreased after treatment with LPA and that YAP/TAZ target genes (*Ankrd1*, *Ccn1*, *Ccn2*, and *Tagln2*) are not induced in these cells because YAP remains phosphorylated in the presence of ROCK inhibitor [45]. We evaluated the protein levels of YAP/TAZ to determine

(See figure on next page.)

**Fig. 4** Fibrotic markers are increased early in *Sgcd*<sup>-/-</sup> mice. **A** Gene expression levels of ECM components (*Fn1*, *Ccn2*, *Col1a1*, and *Col3a1*) and FAPs/active fibroblast markers (*Pdgfra* and *Postn*). Data are normalized to *gapdh* ( $n=3-5$ ). A two-way ANOVA with Tukey's multiple comparison post-test was used to compare genotypes of mice at each age and muscle. Values represent mean  $\pm$  SEM; \* $p \leq 0.05$ , \*\* $p \leq 0.01$ , \*\*\* $p \leq 0.001$ , and \*\*\*\* $p \leq 0.0001$ . **B** Immunoblot analysis of fibronectin, CTGF/CNN2, PDGFR $\alpha$ , periostin, and GAPDH protein levels in TR lysates. Protein levels normalized to GAPDH compared by unpaired two-tailed t-test for mouse genotypes at each age and muscle ( $n=3$ ). Values represent mean  $\pm$  SEM; \* $p \leq 0.05$ , \*\* $p \leq 0.01$ , and \*\*\* $p \leq 0.001$ . **C** Representative images of TR fibrosis visualized by fibronectin immunofluorescence (red) and Hoechst (nuclei, blue) and Sirius Red staining (collagen, red). Scale bar: 100  $\mu$ m



if this pathway is activated in the context of this LGMD (Fig. 6D). In the TR of *Sgcd*<sup>-/-</sup> mice, both proteins were increased at the first month, but only YAP was significant. At the second month, both proteins were significantly increased in this muscle. The pattern in other muscles differed, where only TAZ levels were higher in GST and DFG from *Sgcd*<sup>-/-</sup> mice only at the second month or both ages, respectively. In addition, to assess how YAP/TAZ protein expression may affect the level of transcriptional activity, we measured the gene expression of YAP/TAZ target genes, i.e., *Ankrd1*, *Ccn1* and *Tagln2*, in TR muscle (Fig. 6E). Surprisingly, *Ankrd1* and *Tagln2* gene expression was up-regulated in *Sgcd*<sup>-/-</sup> mice at both ages compared to control mice. No changes in *Ccn1* mRNA levels were detected.

These results show that the ATX-LPA axis and its downstream effectors YAP/TAZ are dysregulated as early as one month of age in delta sarcoglycanopathy.

## Discussion

As a subset of LGMD, sarcoglycanopathies are rare genetic disorders in humans that affect pelvic and shoulder girdle muscles in a highly heterogeneous manner [46]. As no cure has been developed for these diseases, efforts to understand the mechanisms associated with the development of pathology are critical to potentially identify therapeutics that could ameliorate or delay muscle deterioration. This report provides insight into the early dystrophic changes (muscle damage, regeneration, inflammation, fibrosis, and poor muscle mechanics) observed in the animal model of  $\delta$  sarcoglycanopathy (*Sgcd*<sup>-/-</sup>).

Our study shows for the first time detailed early dystrophic features (fibers in degeneration, fibrosis, inflammatory infiltrate) and regeneration (fibers with central nuclei) in *Sgcd*<sup>-/-</sup> mice at 1 month of age in the TR muscle. Although DFG and GST have been used to characterize this animal model, neither muscle has a direct link to the scapular or pelvic girdle. In contrast, the TR is a representative muscle for LGMD due to its direct relationship to the shoulder girdle, having a proximal insertion with the scapula. Regarding DFG and GST, similar findings have been described in animals aged four weeks

and older [6, 11, 47]. These findings provide evidence of early muscle vulnerability in this animal model and that changes can be observed in girdle muscles, such as the TR, and non-girdle muscles (DFG and GST). By the second month of life, these changes become more apparent.

Damage to muscle fibers is the pathophysiological event that initiates the degeneration process [48], since the loss of sarcoglycans destabilizes the muscle fiber against mechanical forces during contraction [5]. As a result of damage progression and impaired regeneration, dystrophic muscle experiences a loss of muscle mass [37]. For instance, muscle biopsies from subjects with sarcoglycanopathy ( $\alpha$ ,  $\beta$ , and  $\gamma$ ) ranging from children to adults have shown higher values of fiber atrophy than controls. This loss of muscle mass has significant consequences, including weakness, increased risk of comorbidities, and impaired exercise capacity [49]. By the second month, it was observed that muscles in *Sgcd*<sup>-/-</sup> mice had smaller fibers than *Sgcd*<sup>+/+</sup>, consistent with other studies [6, 7, 50]. This is evidence that the imbalance between fiber damage and regeneration is not an early phenomenon and that muscles are capable of maintaining their mass during the first month. In addition, the muscles were characterized by increased *Myh3* gene expression and eMHC protein levels at both ages, indicating an early active regeneration process, a capacity that should be preserved with potential treatments. Higher *Myh3* expression in the same muscles (TR, GST, and DFG) was also observed in *Sgca*<sup>-/-</sup> and *Sgcd*<sup>-/-</sup> mice at eight weeks of age [6]. As further confirmation, a significant increase in the percentage of centrally nucleated and eMHC-positive fibers was observed in the TR of *Sgcd*<sup>-/-</sup> mice at both ages. Centrally nucleated fibers have also been described in the *Sgcd* mutant TO-2 hamster at five weeks of age [51] and in 4-month-old *Sgcd*<sup>-/-</sup> mice [47].

Inflammation and fibrosis are critical features of muscle dystrophies. Indeed, dystrophic muscle undergoes exacerbated and recurrent inflammation by activating innate and adaptive immune responses [9] triggered by necrotic and damaged fibers [52]. Consistent with histologic observations of an inflammatory infiltrate, we have shown for the first time that molecular and cellular markers of inflammation are dysregulated in  $\delta$

(See figure on next page.)

**Fig. 5** From an early age, *Sgcd*<sup>-/-</sup> mice have impairments in TA and EDL muscle function. **A** TA isometric force (force-frequency relationship) measured at different stimulation frequencies (1–200 Hz). Mice were compared at different ages using two-way ANOVA with Tukey's multiple comparisons post-test ( $n=5$ ). Values represent mean  $\pm$  SEM; \* $p \leq 0.05$ , \*\* $p \leq 0.01$ , \*\*\* $p \leq 0.001$ , and \*\*\*\* $p \leq 0.0001$ . **B** Fatigue and recovery curves of TA muscle were evaluated using two-way ANOVA with Tukey's multiple comparisons post-test ( $n=5$ ). Values represent mean. **C** EDL specific (N/cm<sup>2</sup>) and normalized (N/g) force at both ages ( $n=3-4$ ). Values represent mean  $\pm$  SEM; \*\* $p \leq 0.01$ . **D** EDL resistance to mechanical damage by ECC stimulation ( $n=3-4$ ). Two-way ANOVA with Šidák multiple comparisons post-test was used to compare mice at each age. Values represent mean  $\pm$  SEM; \* $p \leq 0.05$ , \*\* $p \leq 0.01$ , \*\*\* $p \leq 0.001$ , and \*\*\*\* $p \leq 0.0001$

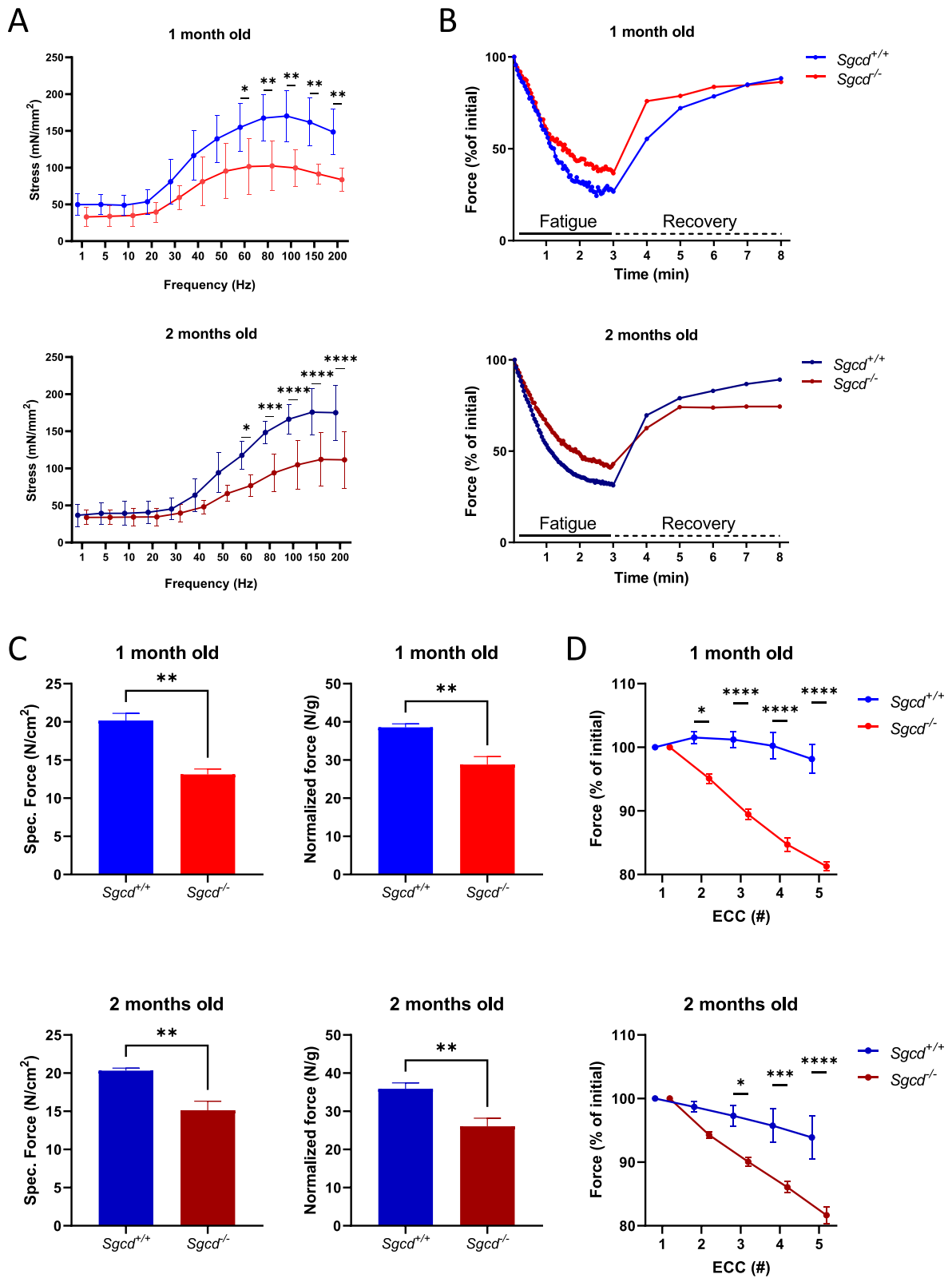


**Fig. 5** (See legend on previous page.)

sarcoglycanopathy. Pro-inflammatory cytokine genes, *tnfa*, *Il1b*, and *Il6*, were significantly higher in *Sgcd*<sup>-/-</sup> mice in all muscles at both ages. These molecules are crucial in recruiting and activating other innate and adaptive immune cells [52]. Similar upregulation in cytokine genes was observed in 4-, 6- and 8-week-old D2.*mdx* skeletal muscle [53, 54]. In addition, changes in genes related to cellular markers (*Ptprc*/CD45, *Ly6c1*, and *Mrc1*) were observed in a muscle- and time-dependent manner. CD45, a pan-leukocyte marker that was up-regulated in our samples, was also found to be higher in the muscle biopsies of patients with *Sgca* and *Sgcg* mutations [52]. Regarding gene expression, only *cd68* is up-regulated in 8-week-old and older *Sgca*<sup>-/-</sup> and *Sgcd*<sup>-/-</sup> mice [6, 7]. Moreover, markers of monocytes/MPs (CD11b) and T cells (CD44) were increased in TR muscle sections from *Sgcd*<sup>-/-</sup> mice. These findings reveal an enhanced early inflammatory response involving molecular and cellular factors of the innate and adaptive immune systems.

A concomitant fibrotic response was also observed in *Sgcd*<sup>-/-</sup> mice from an early stage, revealing a dysregulation in terms of gene and protein expression of key matrix components (fibronectin, CTGF, and collagens) as well as FAPs markers (PDGFR $\alpha$  and periostin). CTGF per se is a factor that can induce muscle damage, inflammation, and a strong fibrotic response [55]. Moreover, FAPs are recognized as one of the relevant cells in the production of ECM components. These cells are increased in several models that have exacerbated fibrosis, such as muscle denervation, muscle damage by BaCl<sub>2</sub> treatment, and dystrophic and neurodegenerative models [56–58]. A relevant role of FAPs in this dystrophic model may be suggested by the increased PDGFR $\alpha$  protein levels observed in *Sgcd*<sup>-/-</sup> mice and by the fact that LPA increases the number of these cells [28] and their profibrotic response [36]. In addition, labeling of fibronectin and collagen by IIF and Sirius Red staining revealed significant remodeling of the muscle structure in the TR muscle at both ages. These results indicate that in response to the damage associated with this LGMD, there is an early

dysregulated activation of reparative mechanisms that ultimately exacerbate fibrosis.

It is worth noting that muscle fibrosis is closely related to and overlaps with inflammation [8]. Both processes have been shown to play a central role in the deterioration of muscle structure [40, 59–61] and reduction in force generation [62]. The present study has demonstrated for the first time that *Sgcd*<sup>-/-</sup> mice have significantly reduced force generation ability at both ages compared to wild-type mice. As in other dystrophic models [54], sarcoglycanopathy has a detrimental effect on TA and EDL muscle performance. TA showed a reduction in force generation as assessed by the force-frequency curve, affecting the strength over 60 Hz of stimulation. Similar findings in the force-frequency curve were observed in *Sgca*<sup>-/-</sup> and *Sgcd*<sup>-/-</sup> mice at 34 weeks of age, but with a decline in force over a wide range of stimulation frequencies (10–180 Hz) [7]. In association with muscle fiber damage, the observed change in ECM composition may be one of the factors negatively affecting force generation. For example, we have described that overexpression of CTGF in TA muscle, with associated changes in ECM components, induces a reduction in force generation at different stimulation frequencies [55]. In addition, EDL in *Sgcd*<sup>-/-</sup> mice had a lower specific and normalized force than wild type mice. This decrease in strength was also seen in B10-*mdx* and D2-*mdx* mice, but was more pronounced in the latter [53]. EDL muscles of *Sgcd*<sup>-/-</sup> mice have a greater force deficit than wild-type mice after ECC, reflecting increased susceptibility to contraction-induced mechanical damage from an early age. Similar susceptibility has been described in the TA muscle of *Sgcd*<sup>-/-</sup> and *Sgca*<sup>-/-</sup> mice at 34 weeks of age [7]. It has been proposed that the loss of strength seen in *mdx* muscle exposed to ECC results from several factors, including sarcolemmal damage, oxidative stress, and cytosolic calcium disruption [63].

ATX is the only enzyme of the ecto-nucleotide pyrophosphatase/phosphodiesterase family (ENPP2) with lysophospholipase D activity capable of synthesizing LPA from extracellular lysophosphatidylcholine [64]. The

(See figure on next page.)

**Fig. 6** A deregulated ATX-LPA axis and YAP/TAZ signaling are present at an early stage in *Sgcd*<sup>-/-</sup> mice. **A** Gene expression levels of ATX (*Enpp2*). Data are normalized to *18s* ( $n=4-5$ ). A two-way ANOVA with Tukey's multiple comparison post-test was used to compare genotypes of mice at each age and muscle. Values represent mean  $\pm$  SEM; \* $p \leq 0.05$ . **B** LPA levels in the triceps muscle ( $n=4$ ). Two-way ANOVA with Šídák multiple comparisons post-test was used to compare mice at each age. Values represent mean  $\pm$  SEM; \* $p \leq 0.05$ . **C** Gene expression levels of LPA receptors. Data are normalized to *18s* ( $n=3-5$ ). Two-way ANOVA with Šídák multiple comparisons post-test was used to compare mice at each age and muscle. Values represent mean  $\pm$  SEM; \* $p \leq 0.05$ , \*\* $p \leq 0.01$ , \*\*\* $p \leq 0.001$ , and \*\*\*\* $p \leq 0.0001$ . **D** YAP/TAZ and GAPDH protein levels in muscle lysates analyzed by immunoblot. Quantification of protein levels normalized to GAPDH was performed by unpaired two-tailed t-test comparing genotypes of mice at each age and muscle ( $n=3$ ). Values represent mean  $\pm$  SEM; \* $p \leq 0.05$  and \*\* $p \leq 0.01$ . **E** Gene expression levels of YAP/TAZ readouts (*Ankrd1*, *Ccn1*, and *Tagln2*) in TR muscle. Data are normalized to *gapdh* ( $n=3$ ). An unpaired two-tailed t-test was used to compare genotypes of mice at each age. Values represent mean  $\pm$  SEM; \* $p \leq 0.05$

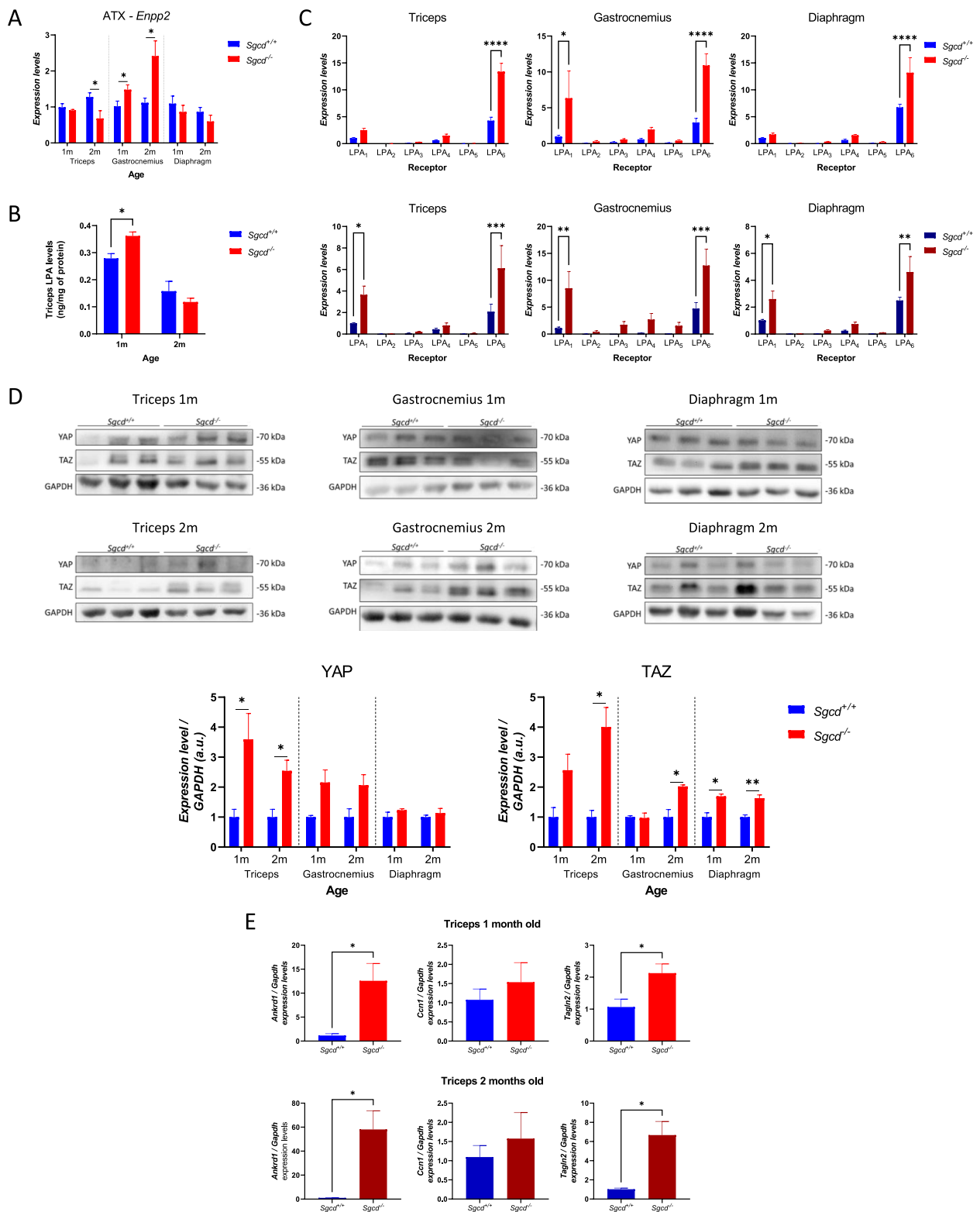


**Fig. 6** (See legend on previous page.)

enzyme and the product have been linked to physiological and pathological processes. ATX-LPA axis signaling is associated with pain, obesity, cardiovascular disease, cancer, fibrosis, and inflammation in various organs, such as the liver, kidneys, lungs, and brain [16, 21–24]. We reported that skeletal muscle expresses components of the ATX-LPA axis and responds to LPA with increased ECM proteins such as fibronectin and CTGF, revealing a potential role in muscle dystrophies [28]. The discovery of an early dysregulation of the ATX-LPA axis in delta sarcoglycanopathy provides evidence for this hypothesis. Unexpectedly, ATX expression was uneven across the muscles and ages analyzed. During the first month of sarcoglycanopathy, an increase in ATX was anticipated, but this was only observed for GST. The lower expression of ATX in TR muscle may be explained by the negative feedback that LPA can exert on ATX [65]. In addition, our study showed for the first time elevated levels of LPA in muscle tissue. The higher levels of LPA in the TR muscle of *Sgcd*<sup>-/-</sup> mice during the first month support the idea of suppressing ATX expression through a feedback loop and a role of this signaling lipid in the context of muscle dystrophy.

Consistent with the expression levels of LPA receptors in muscle, we found that LPA<sub>1</sub> and LPA<sub>6</sub> were up-regulated in *Sgcd*<sup>-/-</sup> mice in a muscle- and time-dependent manner. We have previously shown that FAPs and skeletal muscle lineage cells differentially express components of this axis, suggesting a different physiological role for LPA signaling in these cells [36, 45]. For instance, the LPA-mediated fibrotic response in muscle could be attributed to LPA<sub>1</sub> signaling, as this response is attenuated by Ki16425 (a LPA<sub>1-3</sub> inhibitor) and in LPA<sub>1</sub>-KO mice [28].

We have previously mentioned that YAP/TAZ is an important downstream effector of LPA [44, 66]. As part of the Hippo pathway, YAP/TAZ activity has been implicated in several diseases (i.e. liver, lung, and kidney) associated with fibrosis and inflammation [31–33, 35]. Our results show for the first time that YAP/TAZ protein levels are up-regulated in delta sarcoglycanopathy, a response that depends on the muscle and age analyzed. This dysregulation of YAP/TAZ protein levels has also been reported in denervated muscle (a model of fibrosis in the muscle) and, in particular, in denervated muscle FAPs, which accumulate YAP in their nuclei [30]. It has also been shown that constitutive overexpression of YAP in mouse muscle fibers is associated with skeletal muscle degeneration and loss of fiber cross-sectional area [67]. This suggests an active role of muscle fibers in the degeneration observed in this model, accompanied by FAPs activation. In addition, we have shown in these cells that the induction of CTGF and other YAP/TAZ target genes

can be prevented by LPA-mediated dephosphorylation of YAP [36, 45]. Furthermore, we have shown that dysregulation of YAP/TAZ protein levels affects the transcript levels of its target genes *Ankrd1* and *Tagln2* in *Sgcd*<sup>-/-</sup> mice. Even *Ccn2* (CTGF), another major target gene of YAP/TAZ, was up-regulated in the TR of two-month-old *Sgcd*<sup>-/-</sup> mice. This transcriptional upregulation of YAP/TAZ target genes was also seen in denervated muscle [30].

These data support the idea that the ATX-LPA axis and the YAP/TAZ pathway, like other classical signaling pathways, play a key role in muscle dystrophies and represent a potential target for the development of muscle dystrophy treatments.

Although this is the first descriptive study characterizing the dysregulation of ATX-LPA and YAP/TAZ signaling in delta sarcoglycanopathy, several limitations should be acknowledged. First, the cross-sectional nature of our study prevents us from determining the contribution of ATX-LPA and YAP/TAZ signaling to disease progression. Future mechanistic studies will be needed to fully elucidate their role in disease pathophysiology. Second, we indiscriminately used both female and male mice in our study, which may have masked potential sex-specific differences in ATX-LPA pathway regulation. Third, although we observed reduced fiber size at two months of age, the underlying mechanisms remain to be elucidated. Another limitation is that although we demonstrated increased susceptibility to contraction-induced damage in EDL muscles by ECC, we were unable to perform similar assessments in TA muscles. In addition, ATX and LPA ELISA measurements were limited to the triceps muscle, which may not fully represent the behavior of the pathway in different muscle groups.

## Conclusions

*Sgcd*<sup>-/-</sup> mice appear to be an excellent model for studying dystrophy-related processes because they exhibit dystrophic features, active regeneration, inflammation, fibrosis, and muscle physiological impairment that can be detected at an early stage in girdle muscles, such as the TR, and in non-girdle muscles (GST and DFG). In addition, the model shows early dysregulation of the ATX-LPA axis and the YAP/TAZ pathway, both of which are concomitant with inflammation and fibrosis. *Sgcd*<sup>-/-</sup> mice also provide a unique opportunity to identify and test pharmacological agents that can prevent, reduce or even eliminate the observed pathological features.

## Methods

### Animals

One- and two-month-old (female and male) mice with  $\delta$ -sarcoglycan homozygous mutations (*Sgcd*<sup>-/-</sup>) and

their healthy littermates (*Sgcd*<sup>+/+</sup>) were used for experiments. Hemizygous transgenic mice carrying the mutant  $\delta$ -sarcoglycan gene (B6.129-*Sgcd*<sup>tm1Mcn/J</sup>) were obtained from Jackson Laboratories (Bar Harbor, USA) and provided by FibroGen (USA).

Animals were housed under controlled laboratory conditions (12-h light/dark cycle and  $20 \pm 2$  °C) with food (chow diet) and water ad libitum at the Bioterio Fundación Ciencia y Vida (FCV).

All animal experiments were performed according to protocols approved by the FCV Bioethics and Biosafety Committee (P049/2023) and the Institutional Animal Care and Use Committee (IACUC) of the University of Florida (202108822).

### Muscle strength measurement

The isometric force of the left isolated TA was measured at the optimum muscle length ( $L_o$ ) and stimulation voltage, both determined from micromanipulation of muscle length to generate a maximum isometric twitch force. The maximum isometric tetanic force was determined from the plateau of the frequency–force relationship after ipsilateral sciatic stimulation at 1–200 Hz for 400 ms, with a 2 min rest between stimuli. The TA muscles were then evaluated using a fatigue protocol. The muscles were stimulated at 150 Hz every three seconds for 68 stimuli. Then, five stimuli were delivered every minute as part of the recovery protocol. After measurement, the muscle was excised and weighed. The normalized specific force or stress ( $\text{mN}/\text{mm}^2$ ) was calculated using muscle mass and  $L_o$  [55, 59].

Isolated muscle function of EDL was performed in another group of mice anesthetized with ketamine/xylazine. After removal, the muscles were placed in modified Ringer's solution (119 mM NaCl, 4.74 mM KCl, 3.36 mM  $\text{CaCl}_2$ , 1.18 mM  $\text{KH}_2\text{PO}_4$ , 1.18 mM  $\text{MgSO}_4$ , 25 mM HEPES, and 2.75 mM glucose, pH 7.4, 23 °C) gas-equilibrated with 95%  $\text{O}_2$ –5%  $\text{CO}_2$ . The tendons were tied closely to the myotendinous junction with a 6–0 silk suture (Genzyme Biosurgery, Fall River, Massachusetts) to a fixed support at one end, and to a force transducer (Aurora Scientific Inc., 150A) at the other end [62, 68]. Isometric muscle force was determined by delivering three series of twitch (500 ms and 1 Hz) and tetanus (500 ms and 120 Hz) delivered at  $L_o$ , with 5-min rest periods between stimulation (Aurora Scientific, 701C). The muscles were rested for five minutes before undergoing an eccentric tetanic contraction. A series of five stimuli were delivered at 120 Hz stimulation for 500 ms, with a 10%  $L_o$  stretch imposed in the last 200 ms and five minutes apart. The loss in force was determined between the first (100%) and the subsequent contractions. After the protocol, the muscles were blotted and weighed. The cross-sectional

area (CSA) was determined using the following formula:  $\text{CSA} = \text{mass} / (\text{Lo} \cdot 1.06 \text{ mg}/\text{cm}^3 \cdot (\text{L}/\text{Lo}))$ , where L is fiber length and L/Lo for EDL is 0.45.

### Muscle extraction

Animals were euthanized under anesthetic gas overdose (isoflurane) using a vaporizer, followed by cervical dislocation as previously described [57]. The loss of reflexes confirmed animal death. After cleaning the incision areas, TR, GST, and DFG were excised. Muscles for IIF and Sirius red staining were immediately frozen in isopentane and stored at  $-80$  °C until processing. The contralateral muscles were stored in separate tubes for protein and RNA extraction.

### Protein extraction and Western blot

Immunoblot analyses were performed as previously described [28]. Muscle extracts were obtained by tissue homogenization in 10 volumes of Tris–EDTA buffer (pH 7.4) mixed with protease/phosphatase inhibitors (1 mM PMSE,  $\text{Na}_3\text{VO}_4$ , and NAF) using an Ultraturrax T25 (Labortechnik) at 22,000 rpm. An equal amount of a second buffer (20% glycerol, 4% SDS, and 0.125M Tris, pH 6.8) was added and mixed using a micropipette. Muscle homogenates were then incubated (at 55 °C for 20 min) and centrifuged (at 12,000 g for 10 min) to pellet insoluble material. The samples were stored at  $-20$  °C until use.

Homogenate protein concentration was measured using the BCA Assay kit (Thermo Fisher Scientific, IL, USA), according to the manufacturer's instructions, in a plate reader (Synergy H1, hybrid reader, BioTek). Protein extracts (25  $\mu\text{g}$ ) from the muscle homogenates were subjected to SDS-PAGE and electrophoretically transferred onto PVDF membranes (Millipore, CA, USA). Membranes were blocked with 5% nonfat milk in TBS-Tween (50 mM Tris–Cl pH 7.6, 150 mM NaCl, 0.1% Tween 20) and incubated overnight with primary antibodies (at 4 °C; Table S2). Primary antibodies were detected using horseradish peroxidase-conjugated secondary antibodies (for 1 h at RT). Immunoreactions were visualized with enhanced chemiluminescence SuperSignal West Dura or Femto (Pierce, Rockford, IL, USA) using a ChemiDoc-It HR 410 imaging system (Upland, CA, USA). Western blot densitometric analysis and quantification were performed using the FIJI software (NIH, USA) [69].

### RNA isolation, reverse transcription, and quantitative real-time PCRs

Total RNA was isolated from the muscles using TRIzol reagent (Invitrogen, CA, USA) according to the manufacturer's instructions [70]. A piece of muscle was homogenized with TRIzol, centrifuged, and the supernatant collected. Then, chloroform was added, mixed, and

centrifuged. The supernatant was precipitated with cold isopropanol, and the pellet was washed with 75% ethanol, air-dried (30 min at RT), and suspended in 30  $\mu$ l of nuclease-free water.

For complementary DNA (cDNA) synthesis, the total RNA was subjected to DNase I treatment. Total RNA (1–2  $\mu$ g) with RNase-free DNase I (1  $\mu$ l; D5307, Sigma-Aldrich), RNaseOUT (20 U; 100,000,840, Invitrogen), 10X reaction buffer (1X; R6273, Sigma-Aldrich), and nuclease-free water as needed (BM-0140, Winkler) was incubated at 37 °C for 30 min. To stop the reaction, 1  $\mu$ l of Stop solution (S4809, Sigma-Aldrich) was added and the mixture heated at 65 °C for 10 min. For the reverse transcription reaction, 5XFS First-strand buffer (1X; 28,025,013; Invitrogen), MMLV reverse transcriptase (100 U; 28,025,013; Invitrogen), random primers (0,6  $\mu$ g; 58,875; Invitrogen), RNaseOUT (100 U; 100,000,840; Invitrogen), dNTPs-mix (0.5 mM; R0192; Thermo Scientific), and nuclease-free water (to a final volume of 25  $\mu$ l) were added and incubated at 37 °C for 60 min. Finally, denaturation was performed at 70 °C for 5 min using an Eppendorf Mastercycler Gradient thermocycler. The cDNA was stored at –20 °C until use.

A quantitative real-time polymerase chain reaction was performed using an Eco Real-Time PCR System (Illumina, CA, USA), as previously described [71]. Primers used in this study are listed in Table S3. mRNA expression was quantified using the comparative  $C_q$  method ( $\Delta\Delta C_q$ ), with *18s* rRNA and *gapdh* as housekeeping reference genes. The mRNA levels were expressed relative to the mean expression of the control condition.

### ELISA assay

ATX and LPA levels in the triceps muscle were measured by enzyme-linked immunosorbent assay (ELISA) according to the manufacturer's instructions (#LS-F16526 and #LS-F25111, Lifespan Biosciences, WA, USA).

### Indirect Immunofluorescence

Muscles were sectioned into 8  $\mu$ m slices, fixed in 4% paraformaldehyde for 10 min, and washed in 1X phosphate-buffered saline (PBS). Permeabilization with 0.1% Triton X-100 in PBS was performed for 5 min. Tissue sections were blocked with 1% bovine serum albumin in PBS for 1 h and incubated overnight with primary antibodies (Table S2) at 4 °C. The slices were then washed three times in PBS and incubated with the corresponding secondary antibody (Table S2) at room temperature for 1 h. After three PBS washes, the slices were incubated with Hoechst 33,342 (1:1,000) in PBS for 10 min and mounted with Dako fluorescent mounting medium (S3023) [28].

### H&E and Sirius red stain

H&E staining to assess muscle architecture and histology was performed according to standard procedures.

For interstitial collagen detection, the muscles were sectioned (8  $\mu$ m) and stained with Sirius Red [55]. The slices were fixed in 100% ethanol at 4 °C for 30 min and washed with distilled water for 3 min. Incubation was performed in saturated aqueous picric acid at 50 °C for 60 min, followed by 3 min washes in distilled water. Slices were incubated in 1% picosirius red in saturated aqueous picric acid for 5 min and washed with 2% acetic acid. Finally, the samples were dehydrated in an alcohol battery (from 70 to 100%) and xylol (3 min each step), and mounted using Entellan (Merck, Darmstadt, GE).

### Microscopy and analysis

For H&E and Sirius red, sections were imaged at 10X using bright-field microscopy on a Nikon Eclipse E600. Sirius red images were quantified using Fiji software (NIH, USA) [69]. The percentage of red-stained area (% of total collagen) was measured in the whole muscle section.

For IIF, image acquisition was performed by a blinded operator with epifluorescence microscopy (Zeiss Axio-scope fluorescence microscope). Images were acquired at 10X. The area of fluorescence (%) in the muscle section reconstructions was determined by fixing the color threshold for each antibody and applying particle analysis using the Fiji software (NIH, USA) [69]. In addition, fiber size was measured using the minimal Feret diameter of each fiber from 10X reconstructed images of muscles stained with laminin and Hoechst 33,258, using SMASH [72]. Fibers with an area of <100  $\mu$ m<sup>2</sup> or >10,000  $\mu$ m<sup>2</sup> were excluded from the analysis. The same images were used to count centrally nucleated fibers using SMASH. eMHC-positive fibers were counted using Fiji's BioVoxel plugin.

### Statistical analysis

Statistical analyses were performed using Prism 8 software (Graph Pad Software, CA, USA), and data are presented as mean  $\pm$  SEM. An unpaired two-tailed T-test was used for two-group comparisons. Two-way ANOVA with post-test (Tukey's or Šidák) was used for multiple comparisons. Differences were considered statistically significant at the following *p* values: \**p*  $\leq$  0.05, \*\**p*  $\leq$  0.01, \*\*\**p*  $\leq$  0.001 and \*\*\*\**p*  $\leq$  0.0001.

### Abbreviations

ATX	Autotaxin
CCN1/Cyr61	Cellular communication network factor 1
CD	Cluster of differentiation
CSA	Cross-sectional area
CTGF/CCN2	Connective tissue growth factor/Cellular communication network factor 2

DFG	Diaphragm
DGC	Dystrophin-associated glycoprotein complex
ECC	Eccentric contractions
ECM	Extracellular matrix
EDL	Extensor digitorum longus
eMHC	Embryonic Myosin Heavy Chain
FAPs	Fibro/adipogenic progenitors
FCV	Fundación Ciencia & Vida
GST	Gastrocnemius
H&E	Hematoxylin & Eosin staining
IIF	Indirect immunofluorescence
IL	Interleukin
KO	Knockout
LGMD	Limb-girdle muscular dystrophies
LPA	Lysophosphatidic acid
LPAR	Lysophosphatidic acid receptor
L <sub>o</sub>	Optimum muscle length
MPs	Macrophages
PBS	Phosphate-buffered saline
PDGFRα	Platelet derived growth factor receptor alpha
Sgca	α-Sarcoglycan
Sgcd	δ-Sarcoglycan
TA	Tibialis Anterior
TAZ	Transcriptional co-activator with PDZ-binding motif
TNFα	Tumor necrosis factor alpha
TR	Triceps
YAP	Yes-associated protein 1

## Supplementary Information

The online version contains supplementary material available at <https://doi.org/10.1186/s13395-025-00375-5>.

Supplementary Material 1.

## Acknowledgements

The authors gratefully acknowledge FibroGen for providing the animal model and the FCV Animal Facility for its services. We also thank Dr. Alejandra Álvarez of the Pontificia Universidad Católica de Chile for unrestricted access to the Zeiss AxioScope fluorescence microscope and Ms. Darling Vera and Mr. Eduardo Ramírez for their invaluable technical and administrative assistance.

## Authors' contributions

E.R.B. and E.B. provided reagents and animals. C.G-R., E.R.B., and E.B. designed the experiments. The experiments were performed by C.G-R., A.C-C., J.F-C., M.C-S., F.S.G., and A.B-P. C.G-R. wrote the manuscript. The manuscript was revised by A.C-C., J.F-C., M.C-S., F.S.G., A.B-P., J.C., E.R.B., and E.B. All authors approved the manuscript.

## Funding

FONDECYT 1190144, 1230054 grants and CONICYT AFB170005, AC210009, and FB210008 grants to E.B.; Physiological Assessment Core by NIH P50 AR052646 to E.R.B.; Chilean National Research and Development Agency (ANID)/National Doctorate Fellowship (Doctorado Nacional) 21210650, 21191311, 21170735, 21202486 to C.G-R., A.C-C., M.C-S., and F.S.G., respectively; Vicerrectoría de Investigación y Doctorados de la Universidad San Sebastián PhD Scholarship 0010267181 to J.F-C.

## Data availability

No datasets were generated or analysed during the current study.

## Declarations

### Ethics approval and consent to participate

Not applicable.

### Consent for publication

Not applicable.

## Competing interests

The authors declare no competing interests.

## Author details

<sup>1</sup>Escuela de Kinesiología, Facultad de Ciencias, Pontificia Universidad Católica de Valparaíso, 2340025 Valparaíso, Chile. <sup>2</sup>Escuela de Medicina, Facultad de Medicina, Pontificia Universidad Católica de Chile, 8330025 Santiago, Chile. <sup>3</sup>Centro Científico y Tecnológico de Excelencia, Ciencia & Vida, 8580702 Santiago, Chile. <sup>4</sup>Facultad de Medicina y Ciencia, Universidad San Sebastián, 7510602 Santiago, Chile. <sup>5</sup>Departamento de Neurología, Pontificia Universidad Católica de Chile, 7820436 Santiago, Chile. <sup>6</sup>Applied Physiology and Kinesiology, College of Health and Human Performance, University of Florida, Gainesville, FL, USA.

Received: 12 July 2024 Accepted: 13 February 2025

Published online: 06 March 2025

## References

- Shieh PB. Muscular Dystrophies and Other Genetic Myopathies. *Neurol Clin.* 2013;31(4):1009–29.
- Straub V, Murphy A, Udd B. LGMD workshop study group. 229th ENMC international workshop: Limb girdle muscular dystrophies – Nomenclature and reformed classification Naarden, the Netherlands, 17–19 March 2017. *Neuromuscul Disord.* 2018;28(8):702–10.
- Murphy AP, Straub V. The Classification, Natural History and Treatment of the Limb Girdle Muscular Dystrophies. Vol. 2, *Journal of Neuromuscular Diseases.* IOS Press; 2015. p. 57–19.
- Wicklund MP, Kissel JT. The limb-girdle muscular dystrophies. Vol. 32, *Neurologic Clinics.* W.B. Saunders; 2014. p. 729–49.
- Mercuri E, Bönnemann CG, Muntoni F. Muscular dystrophies [Internet]. Vol. 394, [www.thelancet.com](http://www.thelancet.com). 2019. Available from: [www.thelancet.com](http://www.thelancet.com).
- Verhaart IEC, Putker K, van de Vijver D, Tanganyika-De Winter CL, Pasteuning-Vuhman S, Plomp JJ, et al. Cross-sectional study into age-related pathology of mouse models for limb girdle muscular dystrophy types 2D and 2F. *PLoS One.* 2019;14(8):e0220665.
- Pasteuning-Vuhman S, Putker K, Tanganyika-De Winter CL, Boertje-Van Der Meulen JW, Van Vliet L, Overzier M, et al. Natural disease history of mouse models for limb girdle muscular dystrophy types 2D and 2F. *PLoS One.* 2017;12(8):e0182704.
- Mahdy MAA. Skeletal muscle fibrosis: an overview. *Cell Tissue Res [Internet].* 2019;375(3):575–88. Available from: <http://link.springer.com/https://doi.org/10.1007/s00441-018-2955-2>.
- Raffaghello L, Principi E, Baratto S, Panicucci C, Pintus S, Antonini F, et al. P2X7 Receptor Antagonist Reduces Fibrosis and Inflammation in a Mouse Model of Alpha-Sarcoglycan Muscular Dystrophy. *Pharmaceuticals (Basel).* 2022;15(1):89.
- Tidball JG. Mechanisms of muscle injury, repair, and regeneration. *Compr Physiol.* 2011;1(4):2029–62.
- Coral-Vazquez R, Cohn RD, Moore SA, Hill JA, Weiss RM, Davison RL, et al. Disruption of the sarcoglycan-sarcospan complex in vascular smooth muscle: a novel mechanism for cardiomyopathy and muscular dystrophy. *Cell.* 1999;98(4):465–74.
- Mercuri E, Muntoni F. Muscular dystrophies. Vol. 381, *The Lancet.* Elsevier B.V.; 2013. p. 845–60.
- Choi JW, Herr DR, Noguchi K, Yung YC, Lee CW, Mutoh T, et al. LPA receptors: Subtypes and biological actions. Vol. 50, *Annual Review of Pharmacology and Toxicology.* 2010. p. 157–86.
- Yung YC, Stoddard NC, Chun J. LPA receptor signaling: Pharmacology, physiology, and pathophysiology. Vol. 55, *Journal of Lipid Research.* American Society for Biochemistry and Molecular Biology Inc.; 2014. p. 1192–214.
- Solís KH, Romero-Ávila MT, Guzmán-Silva A, García-Sáinz JA. The LPA3 receptor: Regulation and activation of Signaling pathways. Vol. 22, *International Journal of Molecular Sciences.* MDPI; 2021.
- Yung YC, Stoddard NC, Mirendil H, Chun J. Lysophosphatidic Acid Signaling in the Nervous System. Vol. 85, *Neuron.* Cell Press; 2015. p. 669–82.
- Gustin C, Van Steenbrugge M, Raes M. LPA modulates monocyte migration directly and via LPA-stimulated endothelial cells. *American Journal of Physiology-Cell Physiology [Internet].* 2008;295(4):C905–14. Available

- from: <https://www.physiology.org/doi/https://doi.org/10.1152/ajpcell.00544.2007>.
18. Hayashi M, Okabe K, Kato K, Okumura M, Fukui R, Fukushima N, et al. Differential function of lysophosphatidic acid receptors in cell proliferation and migration of neuroblastoma cells. *Cancer Lett.* 2012Mar;316(1):91–6.
  19. Suckau O, Gross I, Schrötter S, Yang F, Luo J, Wree A, et al. LPA 1, LPA 2, LPA 4, and LPA 6 receptor expression during mouse brain development. *Dev Dyn.* 2019;248(5):375–95.
  20. Kremer KN, Buser A, Thumkeo D, Narumiya S, Jacobelli J, Pelanda R, et al. LPA suppresses T cell function by altering the cytoskeleton and disrupting immune synapse formation. *Proceedings of the National Academy of Sciences* [Internet]. 2022;119(15). Available from: <https://pnas.org/doi/full/https://doi.org/10.1073/pnas.2118816119>.
  21. D'Souza K, Nziroera C, Cowie AM, Varghese GP, Trivedi P, Eichmann TO, et al. Autotaxin-LPA signaling contributes to obesity-induced insulin resistance in muscle and impairs mitochondrial metabolism. *J Lipid Res.* 2018;59(10):1805–17.
  22. Zhao Y, Hasse S, Zhao C, Bourgoin SG. Targeting the autotaxin – Lysophosphatidic acid receptor axis in cardiovascular diseases. *Biochem Pharmacol.* 2019;1(164):74–81.
  23. Tigyí G, Dacheux MA, Lin KH, Yue J, Norman D, Benyó Z, et al. Anti-cancer strategies targeting the autotaxin-lysophosphatidic acid receptor axis: is there a path forward? Vol. 40, *Cancer and Metastasis Reviews*. Springer; 2021. p. 3–5.
  24. McDougall JJ, Reid AR. Joint Damage and Neuropathic Pain in Rats Treated With Lysophosphatidic Acid. *Front Immunol.* 2022;4:13.
  25. Geraldo LHM, Spohr TCL de S, Amaral RF do, Fonseca ACC da, Garcia C, Mendes F de A, et al. Role of lysophosphatidic acid and its receptors in health and disease: novel therapeutic strategies. Vol. 6, *Signal Transduction and Targeted Therapy*. Springer Nature; 2021.
  26. Valentine W, Motohashi N, Yanagida K, Tokuoka S, Kita Y, Takao S, et al. Abstract 2462 Regulation of phosphatidylcholine compositions in dystrophic and regenerating skeletal muscle. *J Biol Chem.* 2024;300(3):106412.
  27. Gallardo FS, Córdova-Casanova A, Brandan E. The linkage between inflammation and fibrosis in muscular dystrophies: The axis autotaxin–lysophosphatidic acid as a new therapeutic target? Vol. 15, *Journal of Cell Communication and Signaling*. Springer Science and Business Media B.V.; 2021. p. 317–34.
  28. Córdova-Casanova A, Cruz-Soca M, Chun J, Casar JC, Brandan E. Activation of the ATX/LPA/LPARs axis induces a fibrotic response in skeletal muscle. *Matrix Biol.* 2022;1(109):121–39.
  29. Moya IM, Halder G. Hippo–YAP/TAZ signalling in organ regeneration and regenerative medicine. Vol. 20, *Nature Reviews Molecular Cell Biology*. Nature Publishing Group; 2019. p. 211–26.
  30. Gallardo FS, Córdova-Casanova A, Bock-Pereda A, Rebolledo DL, Ravasio A, Casar JC, et al. Denervation Drives YAP/TAZ Activation in Muscular Fibro/Adipogenic Progenitors. *Int J Mol Sci.* 2023 Mar 1;24(6).
  31. Liu F, Lagares D, Moo Choi K, Stopfer L, Marinkovi A, Vrbanac V, et al. Mechanosignaling through YAP and TAZ drives fibroblast activation and fibrosis. *Am J Physiol Lung Cell Mol Physiol* [Internet]. 2015;308:344–57. Available from: [www.ajplung.org](http://www.ajplung.org).
  32. Shihan MH, Sharma S, Cable C, Prathigudupu V, Chen A, Mattis AN, et al. AMPK stimulation inhibits YAP/TAZ signaling to ameliorate hepatic fibrosis. *Sci Rep.* 2024;14(1):5205.
  33. Habshi T, Shelke V, Kale A, Lech M, Gaikwad AB. Hippo signaling in acute kidney injury to chronic kidney disease transition: Current understandings and future targets. *Drug Discov Today.* 2023;28(8):103649.
  34. Meli VS, Atcha H, Veerasubramanian K, Nagalla RR, Luu TU, Chen EY, et al. YAP-mediated mechanotransduction tunes the macrophage inflammatory response [Internet]. Vol. 6, *Sci. Adv.* 2020. Available from: <https://www.science.org>.
  35. Wang S, Zhou L, Ling L, Meng X, Chu F, Zhang S, et al. The Crosstalk Between Hippo–YAP Pathway and Innate Immunity. *Front Immunol.* 2020;11:323.
  36. Cruz-Soca M, Faundez-Contreras J, Córdova-Casanova A, Gallardo FS, Bock-Pereda A, Chun J, et al. Activation of skeletal muscle FAPs by LPA requires the Hippo signaling via the FAK pathway. *Matrix Biol.* 2023;1(119):57–81.
  37. Angelini C, Tasca E, Nascimbeni AC, Fanin M. Muscle fatigue, nOS and muscle fiber atrophy in limb girdle muscular dystrophy [Internet]. Vol. XXXIII, *Acta Myologica*. 2014. Available from: [www.musclegenetable.fr](http://www.musclegenetable.fr).
  38. Tidball JG. Regulation of muscle growth and regeneration by the immune system. Vol. 17, *Nature Reviews Immunology*. Nature Publishing Group; 2017. p. 165–78.
  39. Pessina P, Cabrera D, Morales MG, Riquelme CA, Gutiérrez J, Serrano AL, et al. Novel and optimized strategies for inducing fibrosis in vivo: Focus on Duchenne Muscular Dystrophy. *Skelet Muscle.* 2014;4:7.
  40. Smith LR, Barton ER. Regulation of fibrosis in muscular dystrophy. Vols. 68–69, *Matrix Biology*. Elsevier B.V.; 2018. p. 602–15.
  41. Wynn TA. Cellular and molecular mechanisms of fibrosis. Vol. 214, *Journal of Pathology*. 2008. p. 199–210.
  42. Alameddine HS, Morgan JE. Matrix Metalloproteinases and Tissue Inhibitor of Metalloproteinases in Inflammation and Fibrosis of Skeletal Muscles. Vol. 3, *Journal of Neuromuscular Diseases*. IOS Press; 2016. p. 455–73.
  43. Minchew EC, Williamson NC, Readyoff AT, McClung JM, Spangenburg EE. Isometric skeletal muscle contractile properties in common strains of male laboratory mice. *Front Physiol.* 2022;4:13.
  44. Yu FX, Zhao B, Panupinthu N, Jewell JL, Lian I, Wang LH, et al. Regulation of the Hippo–YAP pathway by G-protein-coupled receptor signaling. *Cell.* 2012;150(4):780–91.
  45. Córdova-Casanova A, Cruz-Soca M, Gallardo FS, Faundez-Contreras J, Bock-Pereda A, Chun J, et al. LPA-induced expression of CCN2 in muscular fibro/adipogenic progenitors (FAPs): Unraveling cellular communication networks. *Matrix Biol.* 2024;1(130):36–46.
  46. Thompson R, Straub V. Limb-girdle muscular dystrophies - International collaborations for translational research. Vol. 12, *Nature Reviews Neurology*. Nature Publishing Group; 2016. p. 294–309.
  47. Palma-Flores C, Cano-Martínez LJ, Fernández-Valverde F, Torres-Pérez I, de los Santos S, Hernández-Hernández JM, et al. Differential histological features and myogenic protein levels in distinct muscles of d-sarcoglycan null muscular dystrophy mouse model. *J Mol Histol.* 2023;54(4):405–13.
  48. Dowling P, Swandulla D, Ohlendieck K. Cellular pathogenesis of Duchenne muscular dystrophy: progressive myofibre degeneration, chronic inflammation, reactive myofibrosis and satellite cell dysfunction. *Eur J Transl Myol.* 2023;33(4):11856.
  49. Fanin M, Nascimbeni AC, Angelini C. Gender difference in limb-girdle muscular dystrophy: A muscle fiber morphometric study in 101 patients. *Clin Neuropathol.* 2014;33(3):179–85.
  50. Brunetti B, Bacci B, Abbate JM, Tura G, Paciello O, Vaccaro E, et al. SGCD Missense Variant in a Lagotto Romagnolo Dog with Autosomal Recessively Inherited Limb-Girdle Muscular Dystrophy. *Genes (Basel).* 2023;14(8):1641.
  51. Kato Y, Iwase M, Takagi K, Nishizawa T, Kanazawa H, Matsushita A, et al. Differential Myolysis of Myocardium and Skeletal Muscle in Hamsters With Dilated Cardiomyopathy Beneficial Protective Effect of Diltiazem. *Circulation Journal* [Internet]. 2006;70(11):1497–502. Available from: [http://www.jstage.jst.go.jp/article/circj/70/11/70\\_11\\_1497/\\_article](http://www.jstage.jst.go.jp/article/circj/70/11/70_11_1497/_article).
  52. Panicucci C, Baratto S, Raffaghello L, Tonin P, D'Amico A, Tasca G, et al. Muscle inflammatory pattern in alpha- and gamma-sarcoglycanopathies. *Clin Neuropathol.* 2021;40(6):310–8.
  53. Coley WD, Bogdanik L, Vila MC, Yu Q, Van Der Meulen JH, Rayavarapu S, et al. Effect of genetic background on the dystrophic phenotype in mdx mice. *Hum Mol Genet.* 2016;25(1):130–45.
  54. Hammers DW, Hart CC, Matheny MK, Wright LA, Armellini M, Barton ER, et al. The D2.mdx mouse as a preclinical model of the skeletal muscle pathology associated with Duchenne muscular dystrophy. *Sci Rep.* 2020;10(1):14070.
  55. Morales MG, Cabello-Verrugio C, Santander C, Cabrera D, Goldschmeding R, Brandan E. CTGF/CCN-2 over-expression can directly induce features of skeletal muscle dystrophy. *Journal of Pathology.* 2011;225(4):490–501.
  56. Contreras O, Rebolledo DL, Oyarzún JE, Olguín HC, Brandan E. Connective tissue cells expressing fibro/adipogenic progenitor markers increase under chronic damage: relevance in fibroblast-myofibroblast differentiation and skeletal muscle fibrosis. *Cell Tissue Res.* 2016;364(3):647–60.
  57. Gonzalez D, Contreras O, Rebolledo DL, Espinoza JP, Van Zundert B, Brandan E. ALS skeletal muscle shows enhanced TGF-β signaling, fibrosis and induction of fibro/adipogenic progenitor markers. *PLoS One.* 2017;12(5):e0177649.

58. Uezumi A, Fukada S, Yamamoto N, Ikemoto-Uezumi M, Nakatani M, Morita M, et al. Identification and characterization of PDGFR $\alpha$ + mesenchymal progenitors in human skeletal muscle. *Cell Death Dis.* 2014;5(4):e1186.
59. Gonzalez D, Rebolledo DL, Correa LM, Court FA, Cerpa W, Lipson KE, et al. The inhibition of CTGF/CCN2 activity improves muscle and locomotor function in a murine ALS model. *Hum Mol Genet.* 2018;27(16):2913–26.
60. Rebolledo DL, González D, Faundez-Contreras J, Contreras O, Vio CP, Murphy-Ullrich JE, et al. Denervation-induced skeletal muscle fibrosis is mediated by CTGF/CCN2 independently of TGF- $\beta$ . *Matrix Biol.* 2019;1(82):20–37.
61. Morales MG, Gutierrez J, Cabello-Verrugio C, Cabrera D, Lipson KE, Goldschmeding R, et al. Reducing CTGF/CCN2 slows down mdx muscle dystrophy and improves cell therapy. *Hum Mol Genet.* 2013;22(24):4938–51.
62. Smith LR, Barton ER. Collagen content does not alter the passive mechanical properties of fibrotic skeletal muscle in mdx mice. *Am J Physiol Cell Physiol* [Internet]. 2014;306:889–98. Available from: [www.ajpcell.org](http://www.ajpcell.org).
63. Lindsay A, Baumann CW, Rebbeck RT, Yuen SL, Southern WM, Hodges JS, et al. Mechanical factors tune the sensitivity of mdx muscle to eccentric strength loss and its protection by antioxidant and calcium modulators. *Skelet Muscle.* 2020;10(1):3.
64. Jia Y, Li Y, Xu XD, Tian Y, Shang H. Design and development of autotaxin inhibitors. *Pharmaceuticals (Basel).* 2021;14(11):1203.
65. Ninou I, Magkrioti C, Aidinis V. Autotaxin in pathophysiology and pulmonary fibrosis. *Front Med (Lausanne).* 2018;5:180.
66. Role of TGF- $\beta$ /SMAD/YAP/TAZ signaling in skeletal muscle fibrosis American Journal of Physiology-Cell Physiology. <https://doi.org/10.1152/ajpcell.00541.2024>.
67. Judson RN, Gray SR, Walker C, Carroll AM, Itzstein C, Lionikas A, et al. Constitutive Expression of Yes-Associated Protein (Yap) in Adult Skeletal Muscle Fibres Induces Muscle Atrophy and Myopathy. *PLoS One.* 2013;8(3):e59622.
68. Barton ER, Morris L, Kawana M, Bish LT, Torsell T. Systemic administration of L-arginine benefits mdx skeletal muscle function. *Muscle Nerve.* 2005;32(6):751–60.
69. Schindelin J, Arganda-Carreras I, Frise E, Kaynig V, Longair M, Pietzsch T, et al. Fiji: An open-source platform for biological-image analysis. Vol. 9, *Nature Methods.* 2012. p. 676–82.
70. Acuña MJ, Pessina P, Olguin H, Cabrera D, Vio CP, Bader M, et al. Restoration of muscle strength in dystrophic muscle by angiotensin-1-7 through inhibition of TGF- $\beta$  signalling. *Hum Mol Genet.* 2014;23(5):1237–49.
71. Contreras O, Villarreal M, Brandan E. Nilotinib impairs skeletal myogenesis by increasing myoblast proliferation. *Skelet Muscle.* 2018;8(1):5.
72. Smith LR, Barton ER. SMASH - semi-automatic muscle analysis using segmentation of histology: A MATLAB application. *Skelet Muscle.* 2014;4:21.

## Publisher's Note

Springer Nature remains neutral with regard to jurisdictional claims in published maps and institutional affiliations.